DOI: 10.21062/mft.2026.038 © 2026 Manufacturing Technology. All rights reserved. http://www.journalmt.com

Enhancement of Hot Deep Drawing Die Wear Rate using Artificial Intelligence Lubricant Additive

Zaman Khalil Ibrahim (0000-0002-3761-110X)[1,2], Jafar Keighobadi (0000-0002-1216-4518)[1]
[1]Faculty of Mechanical Engineering, University of Tabriz, Tabriz, Islamic Republic of Iran. E-mail: keighobadi@tabrizu.ac.ir
[2]Kut Technical Institute, Middle Technical University, 10001 Baghdad, Iraq. Email: zmn.khalil@mtu.edu.iq

Currently, lubricant additives represent an effective approach for addressing the increasing industrial demand for enhanced tribological performance and extended service life of forming tools. Graphene-based nanocomposites have shown considerable potential in reducing wear and friction while improving lubricant viscosity and thermal stability. Therefore, this study investigates the tribological performance of graphene-enhanced lubricants containing concentrations of 0, 2, 4, 6, 8, and 10 mg/ml graphene combined with 2 wt. % TiO_2 nano-additives under deep drawing conditions. Experiments were conducted within a temperature range of 25–150 °C and applied loads from 5–50 N. The results demonstrated that the lubricant containing 6 mg/ml graphene exhibited the highest tribological enhancement among all tested concentrations. This concentration achieved approximately 43% improvement in wear resistance, 40% reduction in coefficient of friction, and 35% increase in kinetic viscosity compared with the base lubricant without graphene additives. The superior performance of the 6 mg/ml formulation is attributed to the formation of a more stable protective tribofilm, enhanced load-carrying capacity, improved surface separation, and increased thermal stability under severe operating conditions. Furthermore, the addition of graphene nanoparticles significantly reduced direct metal-to-metal contact and improved lubricant film durability, particularly at elevated temperatures and higher applied loads. To further analyze and optimize the experimental results, an artificial neural network model based on a multilayer perceptron (MLP) architecture was developed using both experimental and simulation data. The artificial neural network (ANN) model demonstrated strong predictive capability for wear rate, coefficient of friction, and viscosity as functions of graphene concentration, temperature, and load. The findings confirm the effectiveness of graphene-enhanced nanolubricants in improving the durability and efficiency of deep drawing dies for industrial applications.

Keywords: Graphene, Deep drawing, Nanocomposite, Lubricant additive, Tribological properties, Friction, Wear, Artificial neural network

1 Introduction

Deep drawing is a widely used manufacturing process that involves a sheet metal blank that is radially drawn into a forming die by a force (mechanical action) of a punch. The process is considered "deep" drawing when the depth of the drawn part exceeds its diameter. Deep drawing dies play a crucial role in this process, their wear and tear over time can significantly impact product quality and production efficiency. To address this issue, the development of advanced lubricants is essential to improve wear resistance and prolong the lifespan of drawing dies [1-3].

Graphene, a two-dimensional nanomaterial with exceptional mechanical, thermal, and lubricating properties, has shown great promise in enhancing the performance of lubricants. This proposal outlines a research project aimed at investigating the potential of graphene-enhanced composite lubricants to improve wear resistance in deep drawing dies while considering the effect of temperature variations [4-6]. In this research, manufacturing and design of deep drawing dies will take from handbook of die design.

The energy losing from wear and friction accompts for 1/3 of the world 's energy wasting, that lead to added energy reserves and challenges for environmental protection. The effects of lubrication technical are necessary to enhance the energy adaptability of mechanical operations, leads to mass failures and improving the serving life of the machine an [7- 9].

The percentage 80% of part or component failure because of tears and wear. [10,11] friction and wear not only effect on machine, lifespan, operation, maintenance of traditional industrial equipment, and part quality, but also effect on human applications, biological and micro-devices [12-14].

When a applied lubricating materials in many fields as aero engines are needed to show continued

lubrication performing cross a broad-based temperature extent, that means it can keep stability of coefficient of friction in environments with different temperatures. The materials of lubricant are very high sensitivity to temperature (i.e.) if used the max. setting temperature of traditional liquid lubricating-materials is often no more than (200°C), while polymer based self-lubricating materials used service temperature is limited specific to about (400°C). But mechanical lubrication more than temperature (400°C) can be carried through solid lubrication only [4,5].

In this search, the range of temperature will use (25, 50,75,100,125,150) ° C to check the effect of thermal properties on nanomaterials with lubricants. Upon no alone coating or solid lubricant, has been happened to be able to keep low coefficient of friction and wear rate cross a comprehensive group of temperatures and under different environmental conditions. Notice that continued lubrication from room-temperature to high-temperature has become a bottle cervix stopping excelling in tribological performances. [15,16].

Graphene demonstrations have very high mechanical strength, high electronic and thermal conductivity, and other nonpareil properties that make it really quaint for many applications [17,18]. They can smoothly penetrate the friction interface involved in the friction process and change the interaction between the friction pairs into the sliding between the sheets, because of the small size of the graphene materials and low interlayer shear force [19,20]. Because nano-graphene particles has high surface activity, they can greatly adsorb to friction surfaces and be a protective and stable three layers film, which practically prevents direct-contact with solid friction surfaces [21]. Due to its strong Van der Waals forces and large specific surface area between its layers, graphene has a slant to rapidly clump together [22]. When adding the graphene particles in the lubricant stay to the bottom, only the top of the lubricant is left with the empty base oil, therefore the wear and friction cannot be reduced. This effect of the serving of the lubricant as dispersion stability is important factor for an excellent lubricant. At the fact of graphene has great potential for numbers applications, also it has some inherent properties such as chemical inertness and no band gap which limit its application [23,24]. Because of this reason, the researchers are studying the function of graphene by reaction with inorganic or organic molecules, chemical modification of graphene's surface and non-covalent interactions [25]. The lubricating characterizations and great mechanical of nanoparticles have attracted great importance and motivates researchers have instituted that nanoparticles used as lubricant additives to significantly improve lubricating performance [26]. There are many types of nanomaterials used such as, materials inorganic or organic nanoparticles (molybdenum, iron, copper/graphene, oxide/graphene, titanium, disulfide/graphene, dioxide/polystyrene etc.), carbon-based nanomaterials such as fullerenes and inclusive of metal based nanoparticles (copper, iron ,copper ,molybdenum disulfide, oxide etc.).Lately the graphene and its-derivatives have seemed as (key materials) for the development of different strategies due to their excellent physical, mechanical , chemical and three layers film properties [21-27].

Additionally, the project will employ artificial neural networks (ANNs) for in-depth analysis of the results. Artificial-intelligence techniques like ANN is used to constitute individual relationship between input and output parameters given to ANN as data driven models. The idealism models which give correct-relationship, and which are near to the target (t) demandable are selected for further optimization. The optimization is checked through (GA) genetic algorithm to estimate the best chosen ANN models are fed as inputs which applied as an objective-function for implementing the optimization [28-31].

Deep Neural Network consist of three principal types: Multi-Layer Perceptrons (MLP), Recurrent Neural Networks (RNN) and Recurrent Neural Networks (CNN). In this proposal will work on the first type MLPs models which are the most famous neural network, which is composed of a series of fully connected.

A number of studies have been conducted on the use of graphene-enhanced nanocomposite lubricants for improved wear resistance. These studies have shown that graphene can improve the tribological properties of lubricants by reducing friction, increasing load-carrying capacity, and preventing adhesion and wear. Recently, many previous studies have used nanoparticles as lubricant additives and showed lubricating mechanisms Therefore scientists are searching and working innovative ways to manufacturing nanocomposite and hybrids of lubricant particles. For example:

- Hettiarachchi et al. [32] used 2D nanocomposites of Al_2O with graphene as new additives in coconut oil to enhance engine performance and concluded the decreasing of friction and wear under a lubricant requires different parameters including temperature, viscosity, pressure and density that resulted clear reductions in the coefficient of friction (COF) 28 % and specific fuel consumption 8 %.
- Miao et al. [33] prepared the film of (Ti_3C_2+GO) nanocomposite by a EPD facile

method and resulted of tribological test indicate that the nanocomposite film deposited under 35V exhibits remarkable friction reduction and wear resistance. Namely, the average COF of Ti_3C_2-GO nanocomposite film is reduced by 76% and the wear volume reduced by 86% respectively, compared with the film without GO. Also, the enhanced tribological properties of (Ti_3C_2+GO) nano-composite films are suggested to be the in-situ formation of tribology film.

- Madkour et al. [34] Studied Multi walled carbon nanotube (MWCN) and graphene nanoplatelets reinforced thermoplastic-poly-biodegradable nanocomposites by using solution casting techniques. The addition of graphene with varied amounts was aimed at enhancing the tribological, mechanical and thermal properties of the nanocomposites. The polymeric nanocomposites appeared very advantages for automotive lubricating purposes, food packaging and oil drilling relevance's.
- Omrani et al. [35] investigated two groups of composite (Al/ graphite with 1%) nanoplatelets, while the other group of composites (Al/graphite 1% / Al_2O_3 2%) nanoparticles. The first group of composites showed (20%) increase in hardness while the other group of composites showed 27% increases in hardness compared to Al pure. The COF coefficient of friction tested at 20N and it showed lower by 22% for Al/graphite with 1% and lower 53% for Al/graphite 1% / Al_2O_3 2% compared to corresponding alloys without graphene materials.
- Zhou et al. [36]. Tested the wear resistance and tribological of Ti6Al4V with multilayer graphene MLG / Ag composites TMAC with different temperature from (25 - 600) °C. The results showed that TMAC obtains better tribological behavior, if comparison with Ti6Al4V alloy and Ti6Al4V-Ag composites under the same condition of 400 °C- 10 N - 0.2 m/s, the TMAC gets the best tribological properties with the wear rate of 7.09 10^{-5} $mm^3N^{-1}m^{-1}$ and COF of 0.24.
- Wang et al. [37] concluded, when the addition of few-layer graphene (FLGs) with in-situ TiC can enhanced the compressive strength of composite materials. Also tested wear resistance of materials under the sliding velocity of (200 r/min) and normal load of (800g) and found the average coefficient of friction and wear rate are 0.63 and 0.73 x $10^{-7}m^3N^{-1}m^{-1}$ respectively, when the weight fraction of FLG was less than 0.6 %.This research aims to develop an intelligent model based on artificial intelligence techniques to predict the failure of deep drawing dies in manufacturing processes. By applying predictive maintenance methods and analyzing data collected from embedded sensors, the model seeks to identify patterns and anomalies that indicate potential failures. Bao et al. [38] studied Mn_3O_4/graphene (Mn_3O_4#G) nanocomposites as additives in lithium grease for heavy-load lubrication. Their results showed that adding 0.1 wt% Mn_3O_4#G reduced the coefficient of friction by 43.5% and wear depth by 86.1% compared with grease containing pure graphene. The improved performance was attributed to the formation of a thin protective tribofilm, the low-shear lubricating action of graphene, and the ability of Mn_3O_4 nanoparticles to fill surface defects, resulting in enhanced friction reduction and wear resistance under high-contact-pressure conditions.

Furthermore, the objective of this research is to investigate and improve the tribological performance of deep drawing dies through the development of a graphene-reinforced nanocomposite lubricant based on SAE-40 oil and TiO_2 nanoparticles. The research aims to evaluate the effects of graphene concentration, operating temperature, and applied load on key tribological characteristics, including wear rate, COF, and lubricant viscosity. In addition, finite element simulation using DEFORM-3D is employed to analyze the deep drawing process and identify critical stress, strain, velocity, and displacement distributions within the die-workpiece system. Furthermore, the study seeks to develop an intelligent predictive framework based on ANN to accurately model and predict tribological behavior under various operating conditions. By integrating experimental investigations, numerical simulation, and artificial intelligence

techniques, the work aims to determine the optimum lubricant formulation capable of enhancing wear resistance, reducing frictional losses, extending deep drawing die service life, lowering maintenance costs, and improving the overall efficiency and productivity of metal forming operations.

2 Experimental Procedure

2.1 Design deep drawing and simulation with Deform 2D program

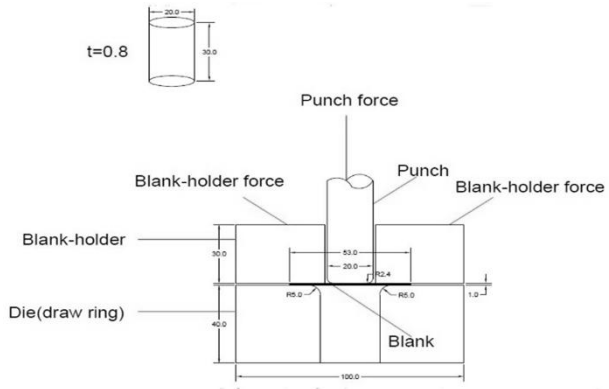


Fig. 1 *Design parts of deep drawing dies and dimension*

Deep drawing dies as shown in figure 1 are designed according to [39][40]. All the fundamentals of deep drawing die design and all details done by 3D-Deform as shown in figure (2). DEFORM-3D is a strong workable simulation regime designed to analyze three-dimensional 3D belch of complicated metal forming processes. DEFORM-3D is an efficient and practical tool to forecast the metal flow in industrial forming operations without the cost, the typical applications include: forging, machining, rolling, drawing, extrusion, compaction, cogging, heading, upsetting. DEFORM based on the finite element process, it has proven to be robust and accurate in industrial application for more than two decades [41].

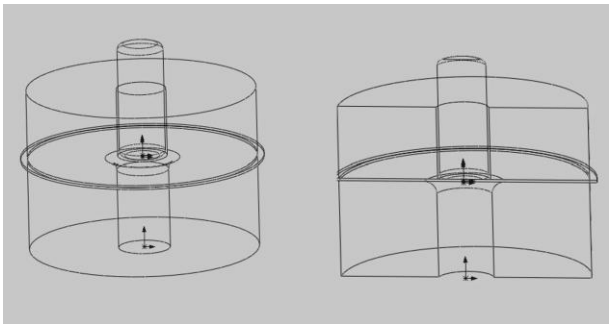


Fig. 2 *Design deep drawing dies and estimate perfect stress-effective by 3D deform*

2.2 Preparation and manufacturing deep drawing die

Manufacturing deep drawing dies from tool steel material (1.2344 according to DIN G X 40 CR MO V 5 1). Table 1 shows classification and nominal compositions of selected tool steel. Original hardness for tool steel was 21 HRC heat treatment of this steel should be made to increase the hardness, the heat treatment was done in Nasr State Company. After that the hardness was measured by Rockwell device, this average hardness was approximately 49HRC. Table 2 shows recommended heat-treating practices for tool steel.

Tab. 1 *classification and nominal compositions of selected tool steel [40]*

Steel	C	Mn	Si	W	Mo	Cr	V	Other
X 40 Cr MO V 5 1	0.35	----	----	----	1.50	5.00	1.00	----

Tab. 2 *Recommended heat-treating practices for hot-work tool steel [40]*

H13 Tool Steel | 1.2344 | X40CrMoV5-1 | SKD61 Hot Work Steel Molybdenum hot work steels										
Type	Rate of heating	Hardening				Holding time, min	Quenching medium	Tempering temperature		Quenched hardness, HRC
		Preheat temperature		Hardening temperature						
		°C	°F	°C	°F			°C	°F	
H13	Moderately from Preheat	815	1500	995-1040	1825-1900	15-40	A or O	540-650	1000-1200	49-53

2.3 Preparation of lubricating oils

Lubrication of SAE-40 oil was Castrol syntil type. Its main properties are shown in table 3. In this search, the graphene was prepared by exfoliation and dispersed in SAE-40 oils. The SEM photo of graphene particles is shown in figure 3. The graphene particles prepared by exfoliation method have relatively complete crystal lattice and a low number of defects. In addition, the particle size of graphene was distributed more intensively and the average particle size of (~ 2-4)μm.

Tab. 3 *Properties of SAE-40 oils*

Property	Value
Kinematic viscosity at 100 °C (cSt)	14.5
Kinematic viscosity at 40 °C (cSt)	109.84
Viscosity index	135
Density at 15 °C (kg/m3)	904
Pour Point (°C)	-27
Flash point (°C)	220

The material used in the present work procured from Sigma, Aldrich /Germany the nanocomposite performance is of great importance on the initial concentration of graphene in lubricant. In this work used many different concentrations of graphene (0, 2, 4, 6, 8, 10) mg/ml + 2% TiO_2 with oil.

Too much graphene can cause agglomeration, making the lubricant non-effective. On the other hand, lower graphene dose would not have the needed improvements in tribological properties. Therefore, to create stable suspension by dispersing graphene nanoparticles in the base lubricant a combination of Ultra sonication and stirring were used as shown figure 4 (a, b). Hence, a preliminary series of experiments were carried out in order to find the optimal amount of graphene to be added to reach the highest performance under deep drawing conditions.

The Raman-spectra of graphene particles can be seen in figure (5) that the intensity of the peak (D) of graphene is lower because the defects of graphene are fewer [7].

Raman spectroscopy is a powerful tool to evaluate the vibrational modes of graphene sheets [41].

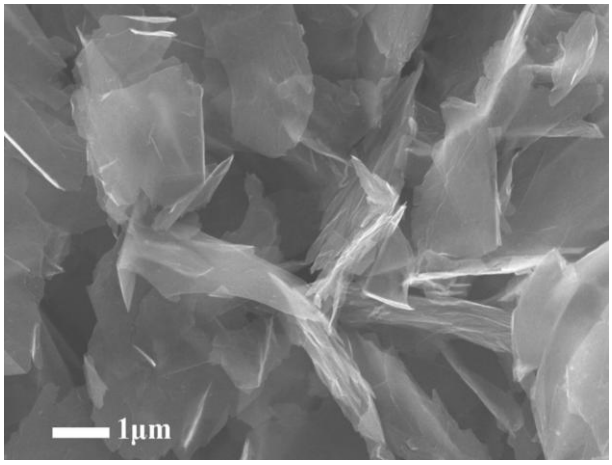


Fig. 3 *Photo of SEM graphene particles*

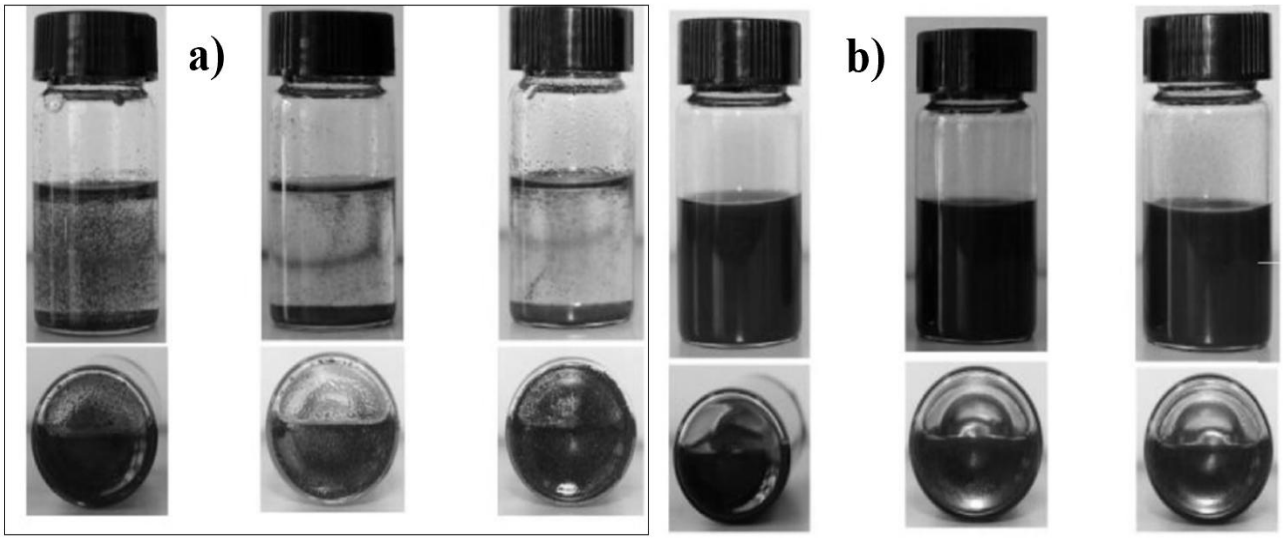


Fig. 4 *(a) The photo of basic oil with nanoparticles of graphene without stirring and ultrasonic treatment at different times, (b) The photo of basic oil with nanoparticles of graphene with stirring and ultrasonic treatment at different times*

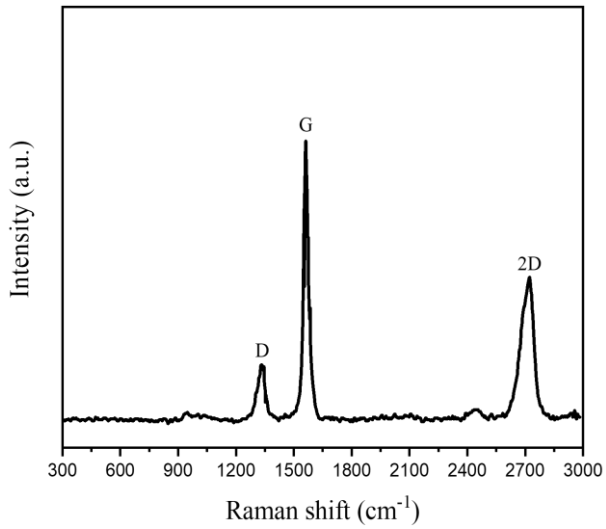


Fig. 5 *Raman-spectra of graphene particles [7]*

2.4 Tribological properties

Wear characteristics of the deep drawing dies, such as surface roughness, weight loss, and microstructural changes, will be analyzed before and after drawing experiments at each temperature condition.

In this work will use (pin on disc) experiment as shown in figure 6 according to ASTM G 99 - 04 standard [42] to measure the wear rate from archard formula. The wear rate is equal to mass loss by sliding distance as shown in figure 7. The COF can be computed from equation (1) [43]:

$$F = \mu N \quad (1)$$

Where:

F, N and μ…The friction force, the normal force and friction coefficient, respectively.

The normal force is load applied during pin on disc experiment in Newton. F is frictional force obtained from the experiment. average of all the readings obtained for the specified distance will give the overall coefficient of friction.

Specific wear rate was calculated with reference to Archard's model by equation (2) [43]:

$$Ws\ (mm^3/Nm) = \Delta V / N \times S \quad (2)$$

Where:

ΔV…The change in volume loss;

N…The normal load;

S…The sliding distance.

In this work experiments were carried out under conditions below, varying the applied load (5, 10, 20, 30, 40 and 50) N at constant speed of 2.355 m/s and sliding distance 1413 m, the duration of each test was 10 minutes, at room temperature.

Shown figure 8 to understand the mechanisms underlying the improved wear resistance achieved by graphene-enhanced lubricants under temperature, force, shape and other parameters variations.

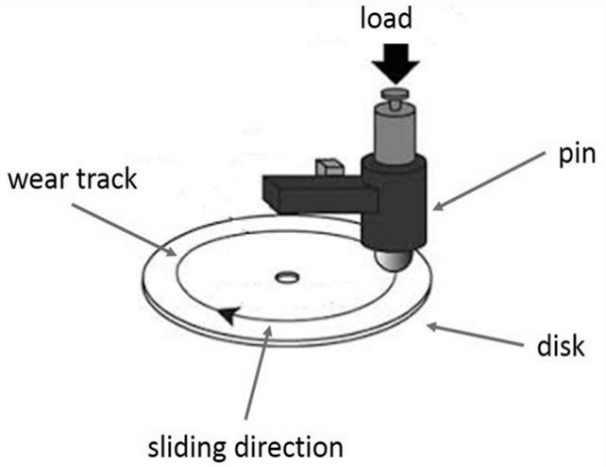


Fig. 6 *Pin on disk experiment*

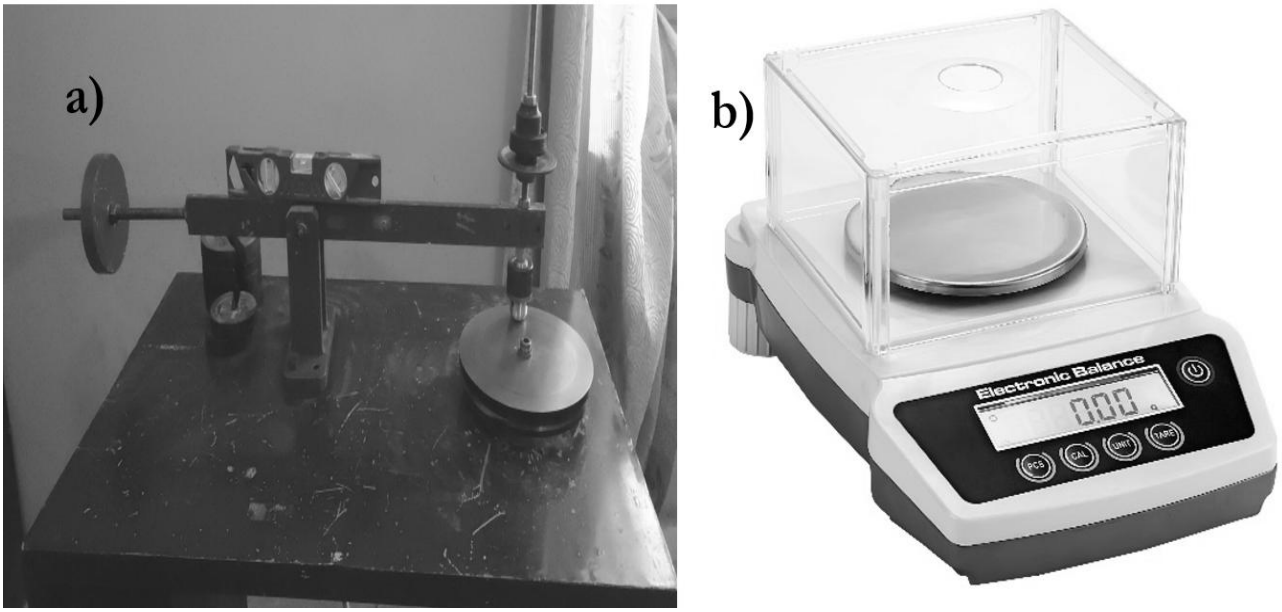


Fig. 7 *a) Wear test equipment and b) sensitive electronic balance*

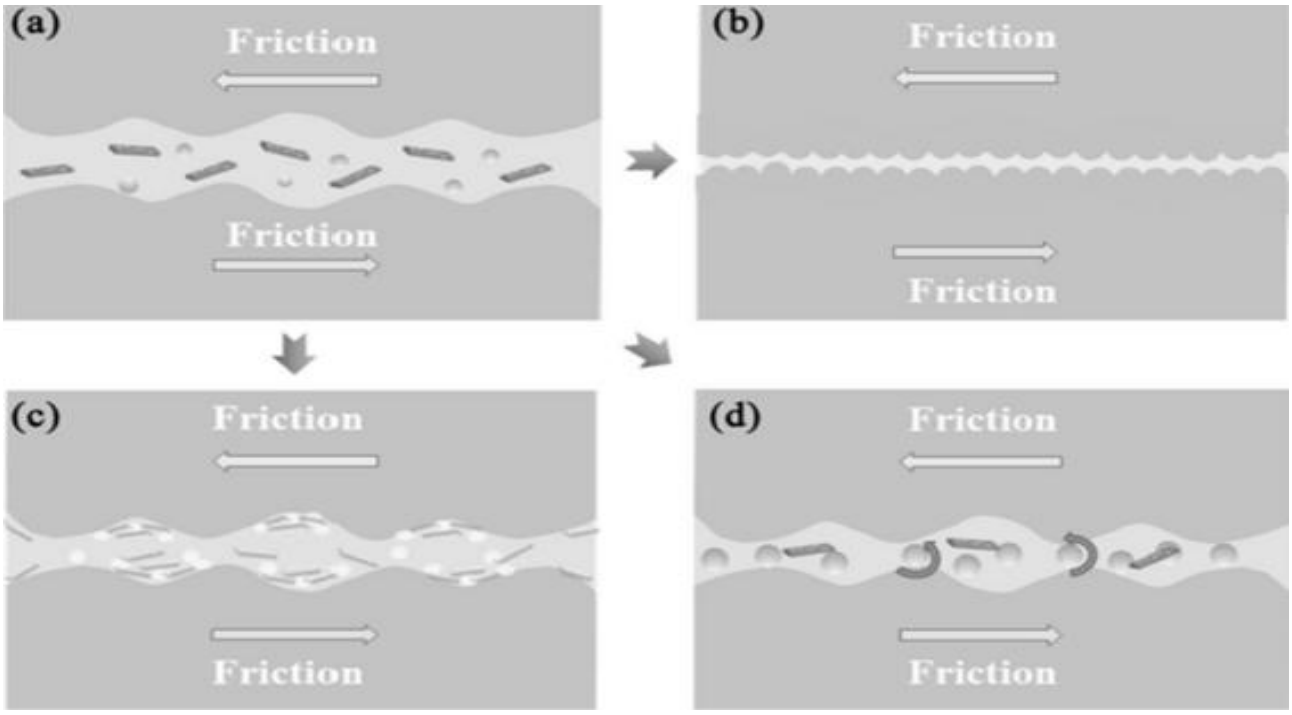


Fig. 8 *Schematic illustration of lubrication mechanisms of graphene-based nanomaterial additives: a) Initial state; b) Forming tribofilm; c) Self-repairing; d) Rolling bearing*

3 Advanced neural network modeling and architecture: integrating theory and practice

This study aims to accurately predict the multi-target properties of nanocomposites, including Wear Rate, COF, and Viscosity, under varying operational conditions, details were descriped in table 4. These properties reflect the complex behavior of materials, and their relationships with input parameters are highly nonlinear. Therefore, a Deep Neural Network (DNN) was employed, as in figure 9 capable of learning complex nonlinear mappings.

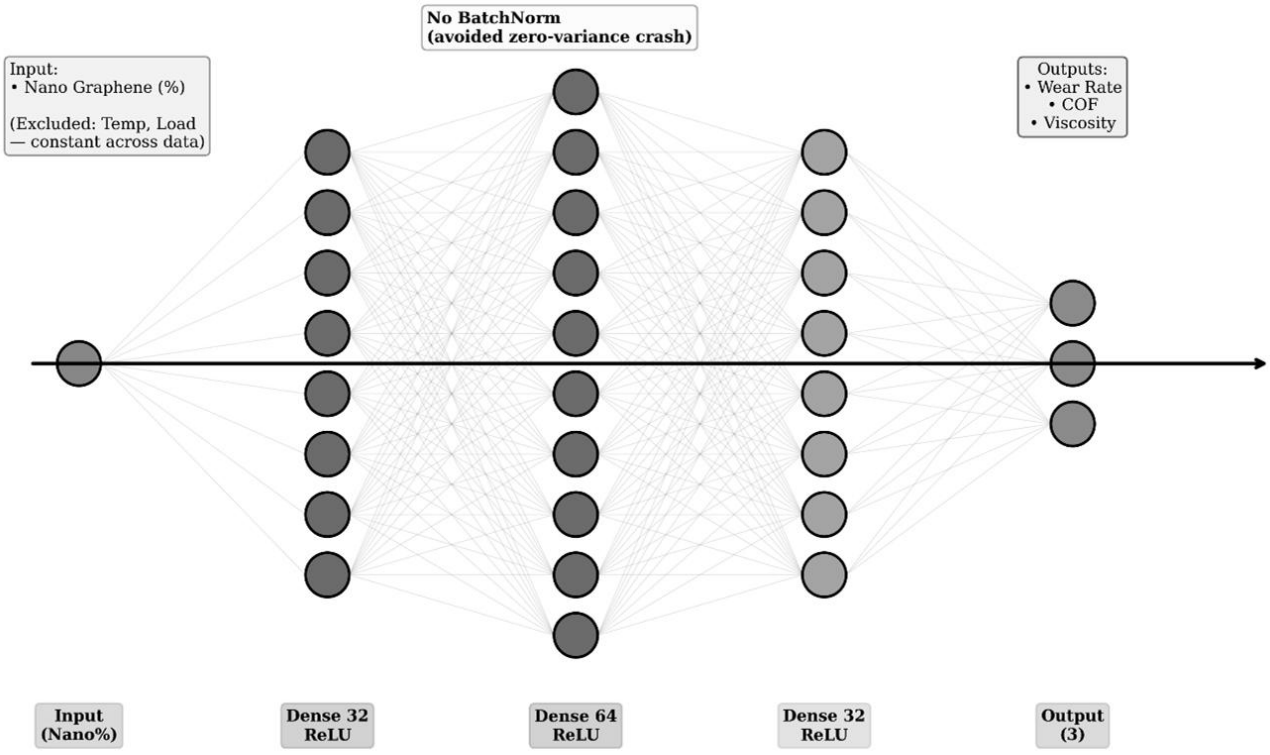


Fig. 9 *Proposed DNN architecture*

3.1 Neurons and dense layers: theory and formulation

Each neuron in the network performs a weighted aggregation of inputs followed by a nonlinear transformation. This process is modeled as:

$$z_i^{(l)} = \sum_{j=1}^{n_{l-1}} w_{ij}^{(l)}\, a_j^{(l-1)} + b_i^{(l)} \tag{3}$$

The ReLU activation function was selected due to its faster convergence and mitigation of the vanishing gradient problem:

$$a_i^{(l)} = f(z_i^{(l)}) = max(\,0, z_i^{(l)}) \tag{4}$$

Nonlinear activation functions enable the network to model complex nonlinear relationships between inputs and outputs. Without them, the network would reduce to a linear model, incapable of accurately predicting material behavior.

3.2 Batch normalization and dropout: stability and generalization

To enhance training stability and convergence speed, Batch Normalization was applied:

$$\hat{a}_i = \frac{a_i - \mu_B}{\sqrt{\sigma_B^2 + \epsilon}}, \quad y_i = \gamma \hat{a}_i + \beta \tag{5}$$

To prevent over fitting, Dropout was incorporated:

$$\tilde{a}_i = a_i \cdot r_i, \quad r_i \sim \text{Bernoulli}(1-p) \tag{6}$$

Batch Normalization reduces internal covariate shift, while Dropout promotes robustness by preventing over-reliance on specific neurons a critical feature in data-limited domains such as nanocomposite modeling.

3.3 Loss function and adam optimizer: precision learning

The network was trained using the Mean Squared Error (MSE) loss function:

$$\mathcal{L}_{\mathcal{MSE}} = \frac{1}{N}\sum_{k=1}^{N}\sum_{i=1}^{3}(y_i^{(k)} - \hat{y}_i^{(k)})^2 \tag{7}$$

The Adam optimizer was used for weight optimization:

$$m_t = \beta_1 m_{t-1} + (1-\beta_1)\nabla_w \mathcal{L}, \quad v_t = \beta_2 v_{t-1} + (1-\beta_2)(\nabla_w \mathcal{L})^2$$
$$\hat{m}_t = \frac{m_t}{1-\beta_1^t}, \quad \hat{v}_t = \frac{v_t}{1-\beta_2^t}, \quad w_{t+1} = w_t - \eta \frac{\hat{m}_t}{\sqrt{\hat{v}_t} + \epsilon} \tag{8}$$

Adam combines adaptive momentum and scaling of gradients, enabling efficient convergence and avoidance of local minima essential for high-dimensional optimization.

3.4 K-Fold cross-validation: generalizability

The model was validated using K-Fold Cross-Validation:

$$\overline{\text{MSE}} = \frac{1}{K}\sum_{k=1}^{K}\mathcal{L}_{\mathcal{MSE}}^{(k)} \tag{9}$$

This technique ensures the model generalizes well to unseen data and is not overfitted to the training set.

3.5 Inverse optimization via differential evolution

After training, Differential Evolution (DE) was used to identify optimal input combinations for desired target outputs:

$$\boldsymbol{f(x)} = \left\|\boldsymbol{y_{pred}(x)} - \boldsymbol{y_{target}}\right\|_{\boldsymbol{2}} \tag{10}$$

New candidate solutions were generated and selected as follows:

$$\boldsymbol{v_i} = \boldsymbol{x_{r1}} + \boldsymbol{F}\cdot(\boldsymbol{x_{r2}} - \boldsymbol{x_{r3}})$$
$$u_{i,j} = \begin{cases} v_{i,j} & \text{if } r_j \le CR \\ x_{i,j} & \text{otherwise} \end{cases}, \quad x_i^{\text{next}} = \begin{cases} u_i & \text{if } f(\mathrm{u}_i) < f(x_i) \\ x_i & \text{otherwise} \end{cases} \tag{11}$$

DE is a global optimization algorithm effective in multi-objective and nonlinear problems. It efficiently explores the complex input–output space learned by the neural network.

3.6 Performance evaluation metrics

R^2 Score measures the proportion of variance explained by the model:

$$R^2 = 1 - \frac{\sum_{i=1}^{N}(y_i - \hat{y}_i)^2}{\sum_{i=1}^{N}(y_i - \bar{y})^2} \tag{12}$$

Mean Absolute Error (MAE) averages absolute prediction error:

$$\text{MAE} = \frac{1}{N}\sum_{i=1}^{N}|\,y_i - \hat{y}_i| \tag{13}$$

These metrics, along with prediction vs. actual plots, provide a comprehensive assessment of model accuracy and reliability.

3.7 Network training dynamics and convergence

With the loss function set as MSE and the optimizer as Adam with a learning rate of $\eta = 0.005$ the neural network was optimized. Two methods were used to validate training convergence:

3.7.1 Leave-One-Out Cross-Validation (LOOCV) Folds

Given the extremely limited dataset size (n = 6 samples), conventional K-fold cross-validation is not appropriate. Therefore, Leave-One-Out Cross-Validation (LOOCV) was adopted, in which n independent training runs are performed. In each run, the model is trained on $n - 1$ samples and evaluated on the remaining held-out sample, ensuring that every sample serves as the validation set exactly once. As shown in Figure 10(a), the cross-validation training trajectories are smooth and stable, exhibiting a consistent exponential decline in the loss function throughout 800 training epochs. This convergence behavior was achieved using an adaptive learning-rate scheduler, which facilitated stable and efficient optimization.

3.7.2 Final Comprehensive Model

The final production model was retrained for 1500 epochs on the full set of data after finalizing hyperparameter settings using LOOCV. It can be seen from figure 10(b) that the primary objective metric (MSE Loss) and secondary validation metric (Mean Absolute Error, MAE) are tightly converged and both are stably reaching their asymptotic floors without oscillations.

Tab. 4 *Experimental tribological test procedure and operating conditions for evaluating graphene-enhanced nanocomposite lubricants under deep drawing applications*

Parameter	Description
Tribological Test Standard	Pin-on-disc tribological test conducted according to ASTM G 99 - 04 standard [42].
Disk Material	Deep drawing die steel material (Tool Steel DIN 1.2344 / H13 hot-work steel).
Pin Material	Hardened steel pin used as counterface material during sliding wear test.
Disk Geometry	Circular rotating disk fabricated from deep drawing die material.
Pin Geometry	Cylindrical pin with hemispherical contact tip used for sliding contact against the rotating disk.
Surface Condition	All specimens were polished and cleaned before testing to ensure uniform surface roughness and remove contaminants. Heat-treated disk specimens had an average hardness of approximately 49 HRC.
Lubricant Condition	SAE-40 oil mixed with graphene nanoparticles (0, 2, 4, 6, 8, and 10 mg/ml) and 2 wt.% TiO_2 nanoparticles.
Graphene Particle Size	Approximately 2–4 μm prepared by exfoliation method.
Test Temperature Range	25 °C, 50 °C, 75 °C, 100 °C, 125 °C, and 150 °C.
Applied Load Range	5 N, 10 N, 20 N, 30 N, 40 N, and 50 N.
Sliding Speed	2.355 m/s.
Sliding Distance	1413 m.
Stabilization time	15 minutes for each experiment.
Wear Measurement Procedure	Wear rate was calculated from Archard's wear equation using mass loss and sliding distance measurements. Mass loss was determined using a sensitive electronic balance before and after testing.
Coefficient of Friction Measurement	COF was calculated from the ratio between friction force and applied normal load during pin-on-disc testing.
Type of viscometer	Ostwald capillary viscometer.
Number of Repetitions	3
Statistical Treatment	Average values of repeated measurements were used for analysis. Standard deviation, MAE, MSE, and R^2 evaluation were employed for ANN validation and uncertainty assessment.
Uncertainty Considerations	±0.5%

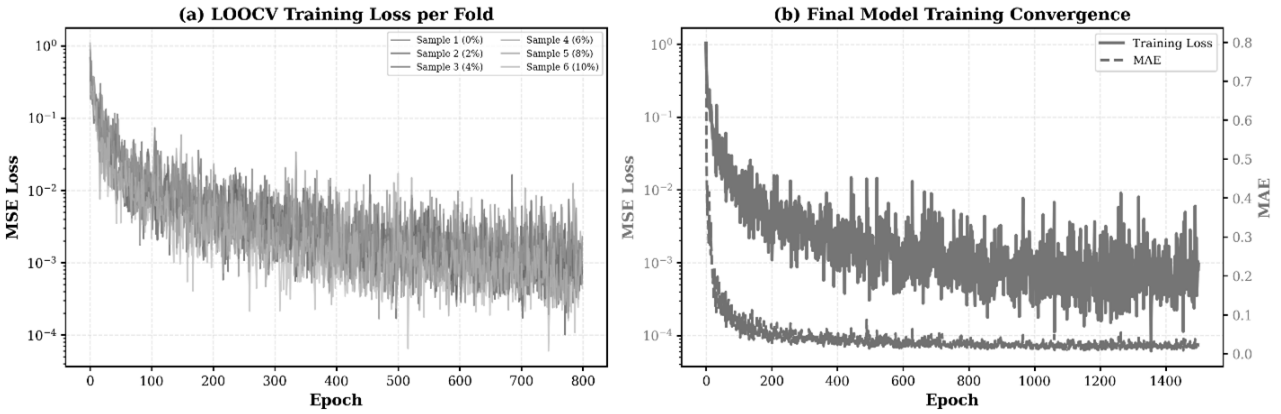


Fig. 10 *Model Training Dynamics*

3.8 Generalization validation via parity plots

The most stringent test of an engine-property network is how it responds to all completely novel inputs. The cross-validated parity plots of the true experimentally derived target vectors vs. the cross-validated network predictions are shown in figure 11.

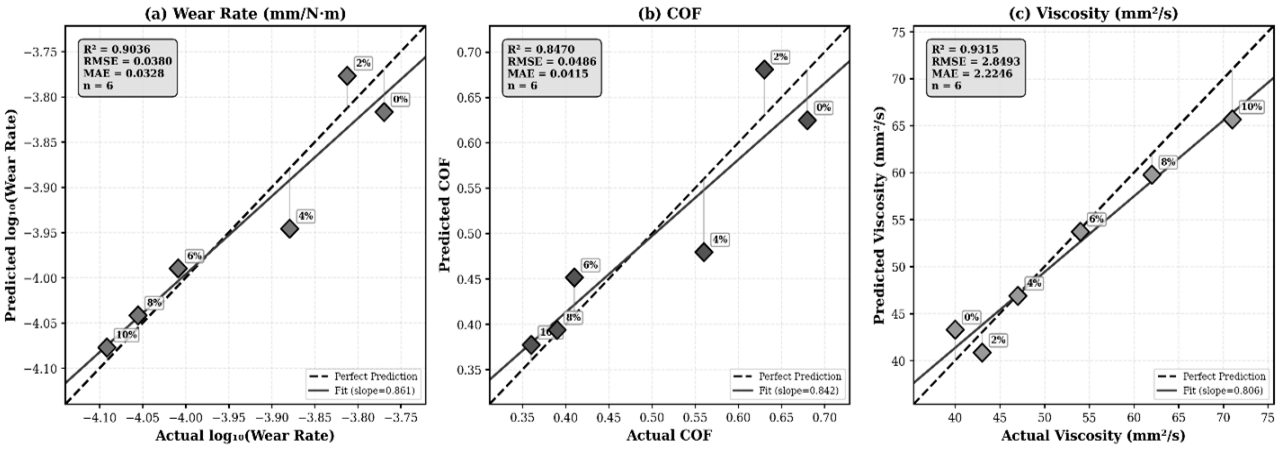


Fig. 11 *Leave-One-Out Cross-Validation Parity Plots*

As Wear Rate is on several orders of magnitude, it is analyzed in log-space log₁₀ (Wear Rate), to ensure balanced error weighting. The quantitative predictive validity of the network is summarized as table 5.

Tab. 5 *The quantitative predictive validity of the network*

Target Performance Output	Coefficient of Determination (R2)	Root Mean Squared Error (RMSE)	Mean Absolute Error (MAE)
log₁₀(Wear Rate)	0.9036	0.0380	0.0328
Coefficient of Friction (COF)	0.8470	0.0486	0.0415
Kinematic Viscosity	0.9315	2.8493	2.2246

The R^2 values for all target categories are above the 0.80 of threshold value recommended for reliable system validation for engineering use with the viscosity models being very close to the "near perfect tracking" value (R^2 = 0.9315). This is a direct confirmation that, although trained on a small network, the custom constraints (drop out Batch Normalization and fixing the dimensions) were able to capture the physical relationships without memorizing noise.

3.9 Residual diagnostics and error distribution

A detailed diagnostic study of the residuals was conducted to check for systematic errors in the prediction errors in the fitted network, by plotting the prediction error against the corresponding fitted output and according to the individual sample categories. As seen in figures 5(a), 5(b) and 5(c), the prediction error value of each point is uniformly distributed around the line of zero error. The data

points still stay within the gray horizontal confidence channels at 1σ around the standard, suggesting that the error variance is homoscedastic and that there is no structural distortion in the errors.

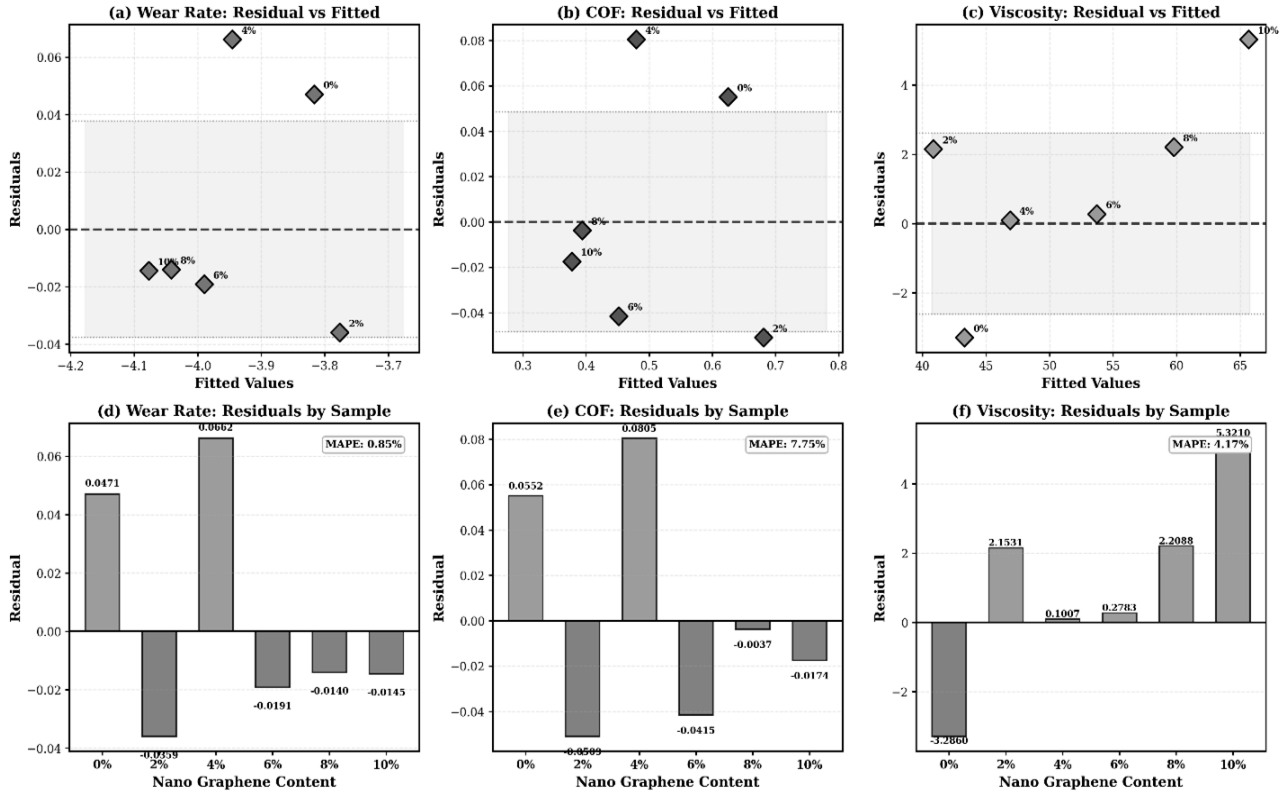


Fig. 12 *LOOCV Residual Analysis*

The total error tracking of the bar metrics for the three models is very low as seen in figures 12(d),(e) and(f).

The MAPE for Wear Rate is 0.85%, which is a good value.

- The standard deviation of Kinematic Viscosity is 4.17%.
- The COF output model records a MAPE of 7.75%. All are within extremely close tolerance required for high precision engineering use.

4 Result and Discussion

4.1 Deform software results

A primary simulation was performed to predict the maximum deep drawing load and other conditions. Figure 13 presents the effective strain-rate and effective strain distributions during the deep drawing process. The maximum effective strain rate reached approximately 0.324 s^{-1} and was concentrated at the die radius, indicating that the highest deformation rate occurred in the bending and unbending zone. Most regions of the workpiece exhibited strain-rate values below 0.108 s^{-1}, reflecting stable material flow. The effective strain distribution shows a maximum value of approximately 1.24 mm/mm at the die corner, while the strain gradually decreased along the cup wall to about 0.80 mm/mm and further decreased toward the flange region. The smooth strain gradient and absence of localized extreme values indicate uniform plastic deformation and successful material flow during the deep drawing operation without signs of excessive thinning or fracture.

The effective strain-rate contour (Fig. 14a) shows that deformation was concentrated mainly in the die radius region, where the maximum strain rate reached approximately 0.324 s^{-1}, while the remaining areas experienced significantly lower values close to zero. This indicates that plastic deformation occurred primarily at the sheet bending and unbending zones, which is consistent with the expected material flow behavior during deep drawing. The effective strain distribution further demonstrates that the highest strain values were concentrated along the die corner and flange transition regions, reaching approximately 1.24 mm/mm, whereas the straight wall regions exhibited much lower strain levels. Such a distribution confirms that the die radius is the most critical location for material deformation and potential thinning. At the same time, the strain remained relatively uniform throughout the formed wall, indicating good material flow and a reduced likelihood of localized necking or fracture.

The maximum principal stress contours shown in Figures 14b and 15a indicate that the stress values ranged between approximately −275 MPa and +275 MPa. The highest tensile stresses were concentrated near the die entry radius and punch contact region, while compressive stresses were distributed along the flange area. The absence of stress concentrations exceeding the material strength suggests that the selected process parameters were appropriate and that the component could be formed successfully without cracking. Furthermore, the smooth stress gradients observed across the workpiece indicate stable load transfer during the forming operation.

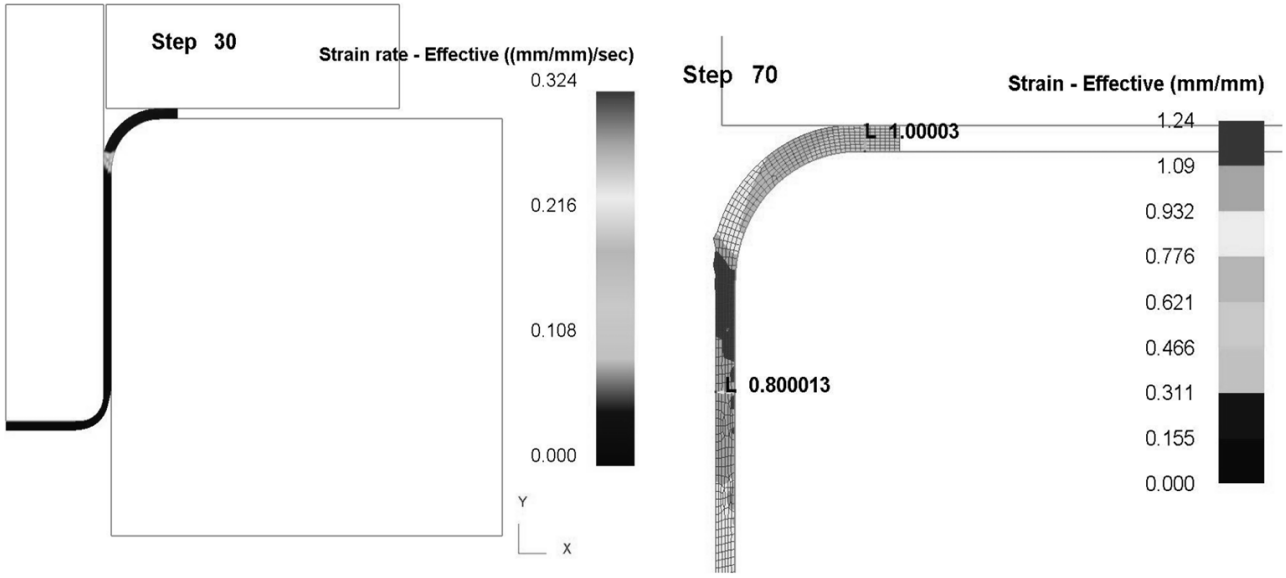


Fig. 13 *Contour plots for different distributions and conditions for deep drawing die*

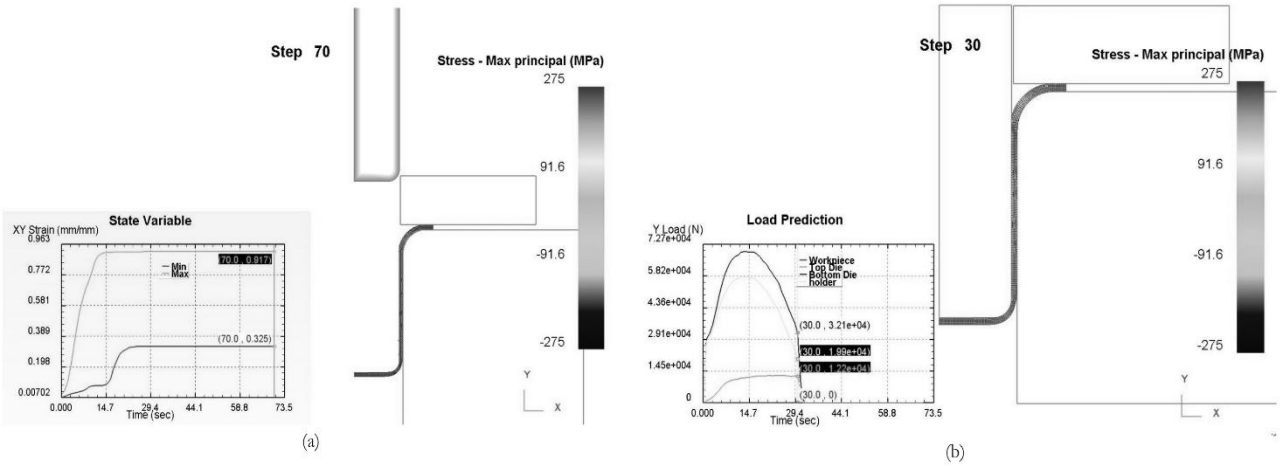


Fig. 14 *(a) Effective strain rate contour plot during the deep drawing process; (b) Max. principal stress contour plot during the deep drawing process*

The velocity contour results (Fig. 15b) reveal that the maximum material flow velocity reached approximately 0.95–1.0 mm/s during the main stage of deformation. The velocity remained nearly constant for most of the forming cycle before gradually decreasing to zero as the punch approached the final position. This behavior demonstrates a stable material flow pattern and confirms that the sheet metal was drawn into the die cavity without severe flow restrictions or instability.

Figure 16 illustrates the displacement distribution during the deep-drawing process at Step 70. The maximum displacement reached 30.2 mm, corresponding to the punch-driven region, whereas the minimum monitored displacement was 8.99 mm. The displacement increased almost linearly during the first 29.4 s of forming and then remained nearly constant, indicating completion of the drawing stroke. The smooth displacement history and absence of abrupt fluctuations confirm stable material flow and successful cup formation without localized failure. The displacement pattern is consistent with the strain and stress concentrations reported near the die radius, where the highest plastic deformation occurs.

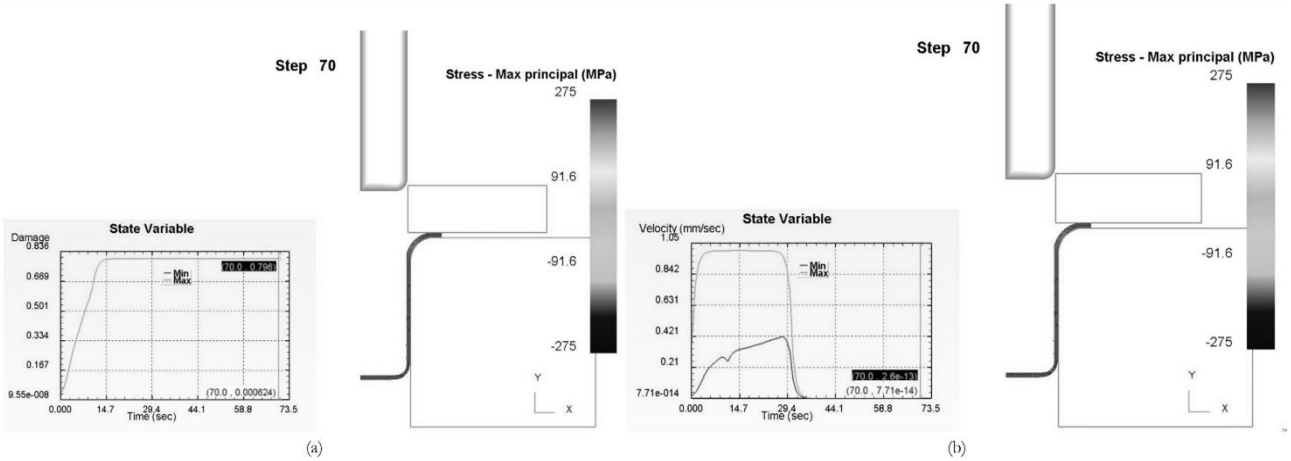


Fig. 15 *(a) Effective stress contour plot during the deep drawing process; (b) Velocity contour plot during the deep drawing process*

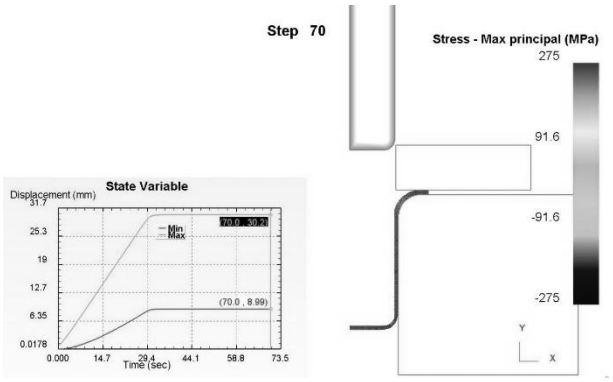


Fig. 16 *Displacement contour plot during the deep drawing process*

4.2 Effect nanoparticles of graphene on tribological properties

The experimental results of applying graphene-enhanced nanocomposite lubricants under deep drawing conditions demonstrated a significant influence of graphene concentration, load and temperature on tribological performance, particularly in terms of wear rate, coefficient of friction and viscosity.

In the base condition with no graphene added (0 mg/ml) and at the room temperature of 25°C, the result was recorded: (1.7×10^{-4} mm³/N.mm) wear rate, (0.68) coefficient of friction and (40 mm²/s) viscosity. When the graphene concentration added to (2, 4, 6, 8 and 10 mg/ml) with fixed other condition (25 °C and 5N), that lead to the wear rate and COF are lower than used oil without graphene nanocomposite, but viscosity is higher than used oil without graphene nanocomposite as shown in figures 17, 18 and 19. Addition of nanographene to lubricant cause this improvement of wear rate percentage of (10%, 23%, 43%, 49% and 53%) respectively, also improvement of COF percentage of (8%, 18%, 40%, 43% and 47%) respectively and improvement of kinetic viscosity percentage of (8%, 18%, 35%, 55% and 78%) respectively.

Nano-graphene particles composite with particle size less than 10μm note improved frictional and wear properties. This material can use the production of friction byproducts to analyze the performance of enhanced oil. They concluded that this property(nanoparticles) is caused by graphene- layers being sheared off to create the tribo-film, where thinner initial graphite creates a more uniform layer of graphene, which in turn improves lubrication [41,43,44].

In contrast, viscosity exhibited a proportional increase with higher graphene concentration. This indicates graphene role in enhancing the lubricant's ability to maintain a stable film under severe conditions.

While one might expect graphene to continuously improve lubrication, the data revealed that exceeding optimal nanoparticle concentration may lead to agglomeration, degrading lubrication performance. This aligns with recent literature suggesting that excessive graphene content causes heterogeneous layers that may increase, rather than decrease, surface wear.

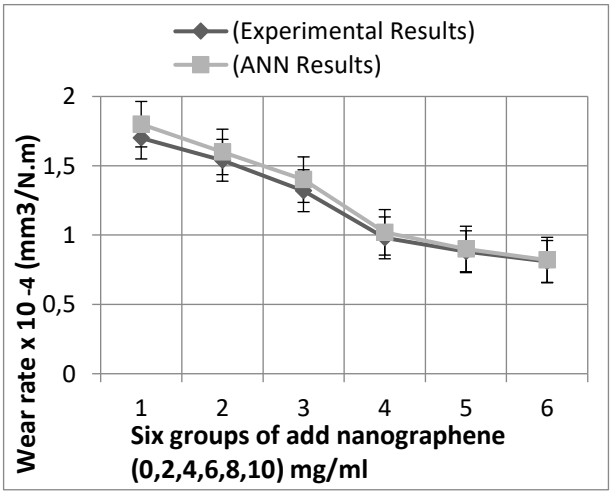


Fig. 17 *Effect the concentration of nano graphene on wear rate*

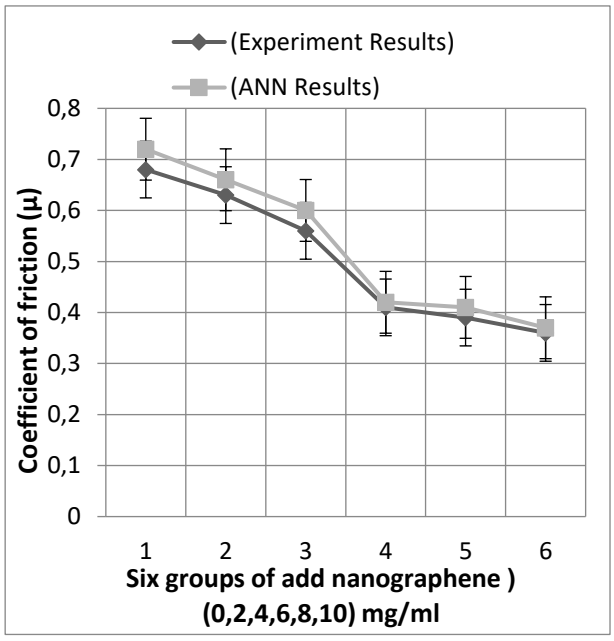


Fig. 18 *Effect the concentration of nano graphene on COF*

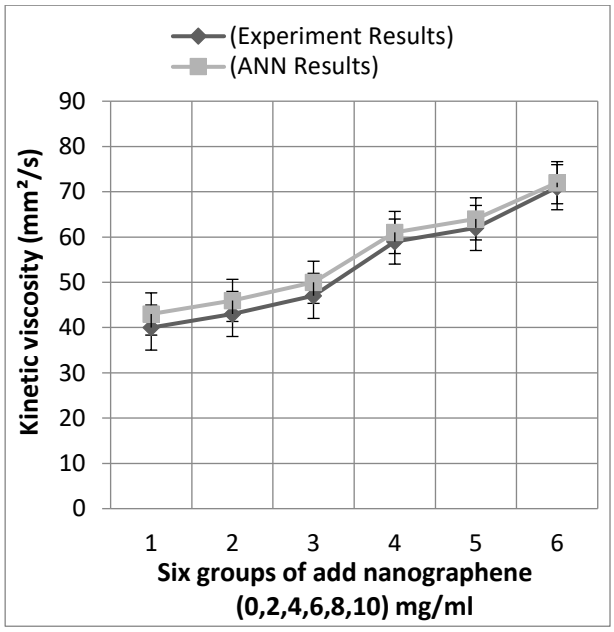


Fig. 19 *Effect of concentration of nano graphene on kinetic viscosity of oil*

The results demonstrated that increasing graphene concentration from 0 to 6 mg/ml significantly improved the tribological properties of the lubricant. At 6 mg/ml, the lubricant exhibited the optimum balance between wear resistance, friction reduction, and viscosity enhancement. This improvement is attributed to the uniform dispersion of graphene nanoparticles and the formation of a stable protective tribofilm that minimized direct surface contact. Although further increases in graphene concentration to 8 and 10 mg/ml resulted in additional viscosity enhancement, no significant improvement in wear rate and coefficient of friction was observed. This behavior can be attributed to nanoparticle agglomeration, reduced dispersion stability, and non-uniform particle distribution within the lubricant. Therefore, 6 mg/ml was identified as the optimum graphene concentration for achieving the best overall tribological performance under the investigated conditions.

4.3 Effect of temperature on tribological properties

After found the perfect addition of enhancement material, we changed the other parameter such as temperature was raised from 25 °C to 50°C, 75°C, 100°C, 125°C and 150°C respectively with fixed (load 5N and 6 mg/ml of nanographene) and compared all result without add any graphene (0 mg/ml). As shown in figures 20, 21 and 22 the added nanoparticles of graphene in oil to lubricant deep drawing dies lead to improve tribological properties, efficiency and durability of these components by decreasing the wear rate and COF and increased the viscosity of oil, although raised the temperature reach to 150°C.

Under certain conditions the researchers found that though the oil carries out well at moderate temperatures, it was outperformed at both high and low temperatures by other nano additives [45,46].

As the friction surface temperature rises, the mechanical activation energy also increases. With the continuous increase of local temperature and surface stress in the friction pair, nanoparticles begin to interact. The micro-asperities on the friction surfaces generate nanostructures that form a thin chemical film with low shear strength and a low COF. In addition, nano-oxidation and gradual oxidation processes create dense nano-films, which also exhibit very low COF. Together with the physically adsorbed layer, these chemical reaction films form an extreme-pressure anti-wear repair layer. This repair layer modifies the surface contact conditions, suppressing furrowing, adhesion, and fatigue wear, while enhancing the load-bearing capacity and improving anti-wear and anti-friction properties of the friction pair. Under higher loads, the friction pair operates in a mixed lubrication regime, combining both fluid lubrication and boundary lubrication [47].

The experimental results demonstrate an increase in temperature decreases viscosity; however, the incorporation of performance-enhancing additives mitigates this effect and improves the surface's physical characteristics under thermal condition. These findings underscore the necessity of identifying a critical balance point between graphene concentration and temperature to achieve optimal performance. The results also provide a basis for developing AI-based predictive models for industrial applications.

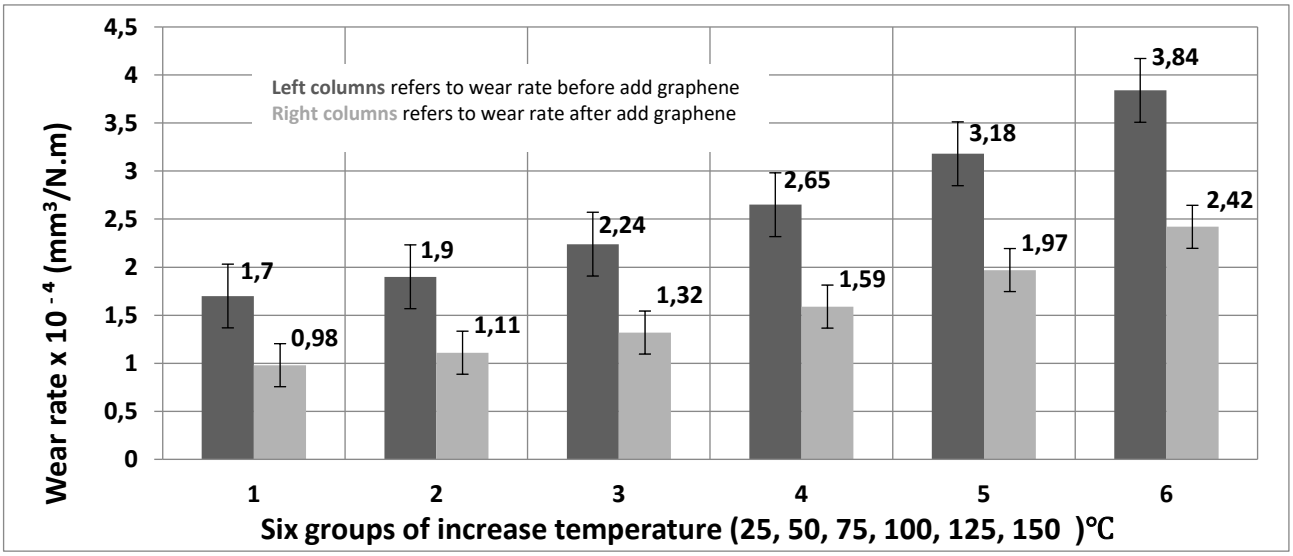


Fig. 20 *Results compare of wear rate between before and after addition nano-graphene, when the temperature rose*

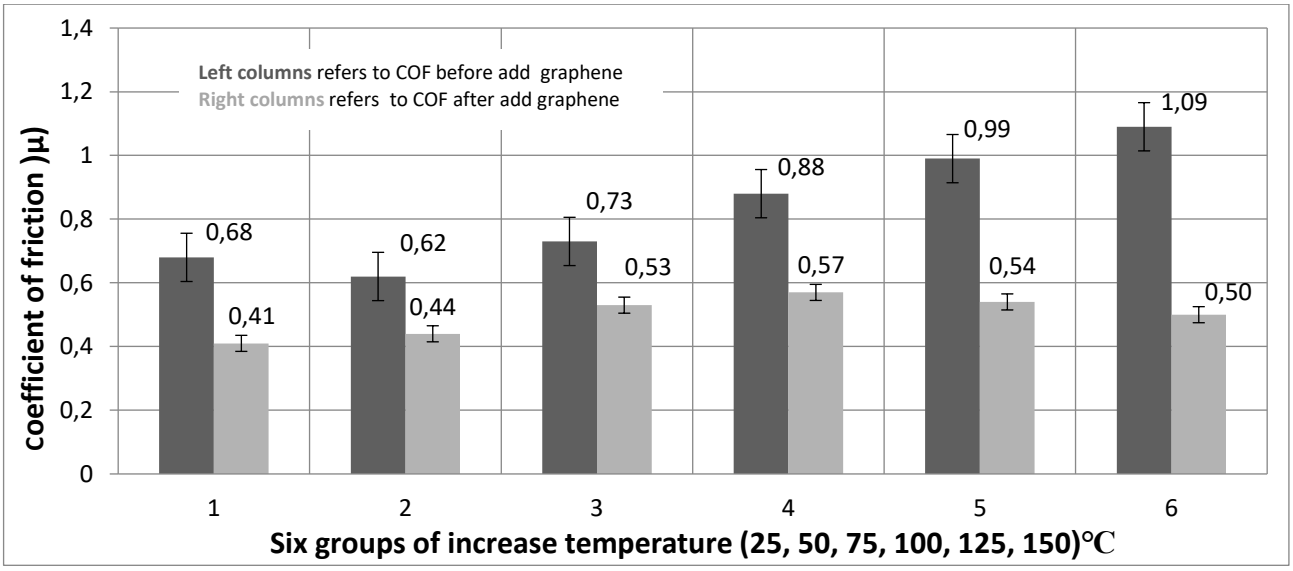


Fig. 21 *Results compare friction coefficient between before and after addition nano-graphene, when raised the temperature*

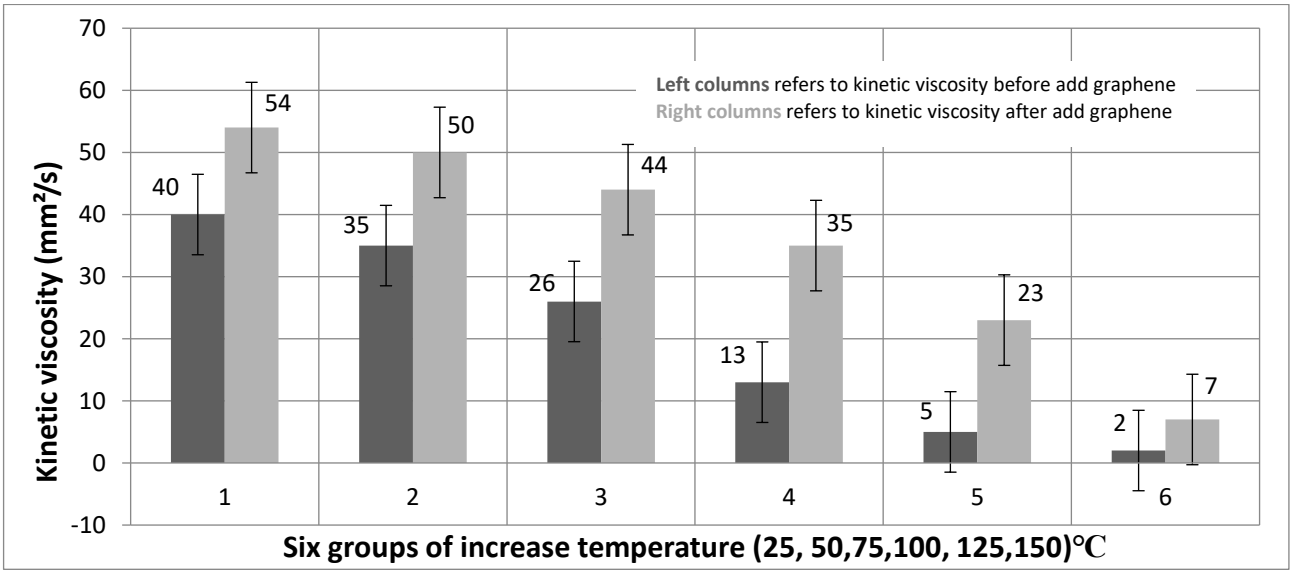


Fig. 22 *Results compare kinetic viscosity between before and after addition nano-graphene, when raised the temperature*

4.4 Effect of load on tribological properties

The third parameter was changed such as load from 5N to 10N, 20N, 30N, 40N and 50N respectively with fixed other parameters (temperature 25°C and 6 mg/ml of nanographene) and compared all results without adding any graphene (0 mg/ml). As shown in figures 23, 24 and 25 the added of nanoparticles of graphene in oil to lubricant deep drawing dies lead to improve tribological properties, efficiency and durability of these components by decreased the wear rate and COF and increased the viscosity of oil, although raised the load reach to 50N.

The tribological properties of the six samples were investigated under four different loads from 5N to 50N. All experiments were repeated three times, and the computed average values were used to plot the figures. We notice two phenomena in the below figures; the first phenomenon is the increase in the wear rate begins from 5N load until reach to 50 N load. The second phenomenon is the decreasing of the wear rate by addition of nanoparticles of graphene. That means the wear rate and COF increased gradational, when increased load but the addition of nanographene exhibit an inverse behavior, as they effectively reduce wear rate and COF even under increased loads, thereby mitigating the adverse impact of the applied load [48].

So, addition of graphene matrix to oil enhances the wear resistance and decreases the coefficient of friction. This may be attributed to the lubricant nature of nanoparticles of graphene. Also, this material has its own high hardness and excellent load bearing capacity which is mainly due to the good connection and better bonding between them [49-52].

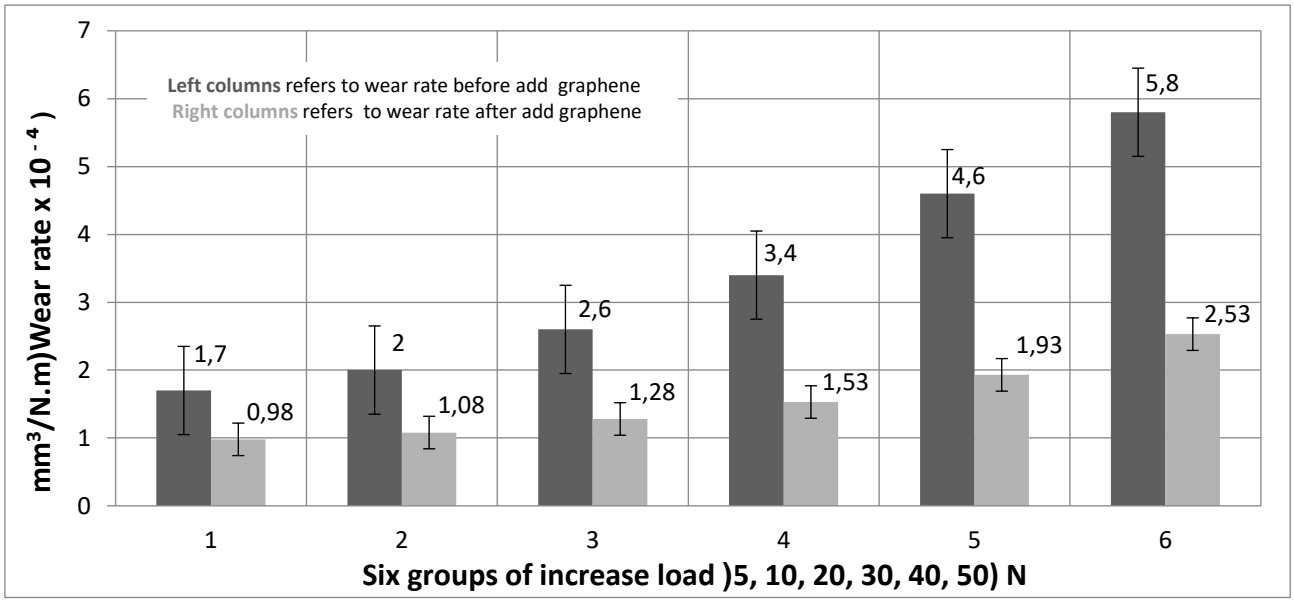


Fig. 23 *Results compare of wear rate between before and after addition nano-graphene, when raised the load*

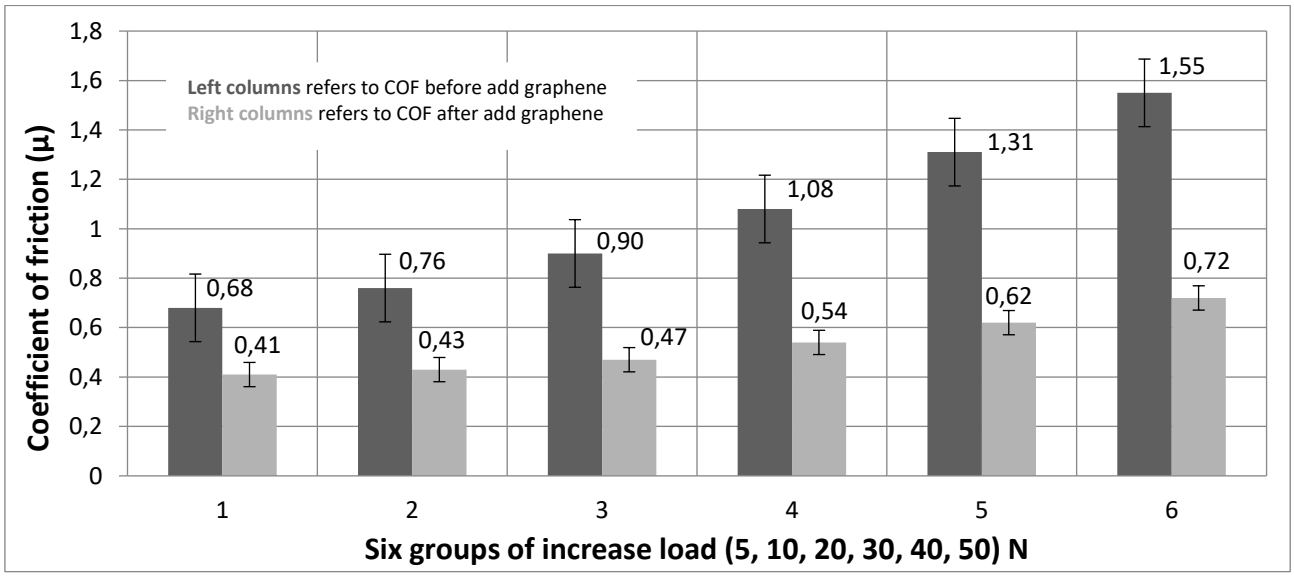


Fig. 24 *Results compare friction coefficient between before and after addition nano-graphene, when raised the load*

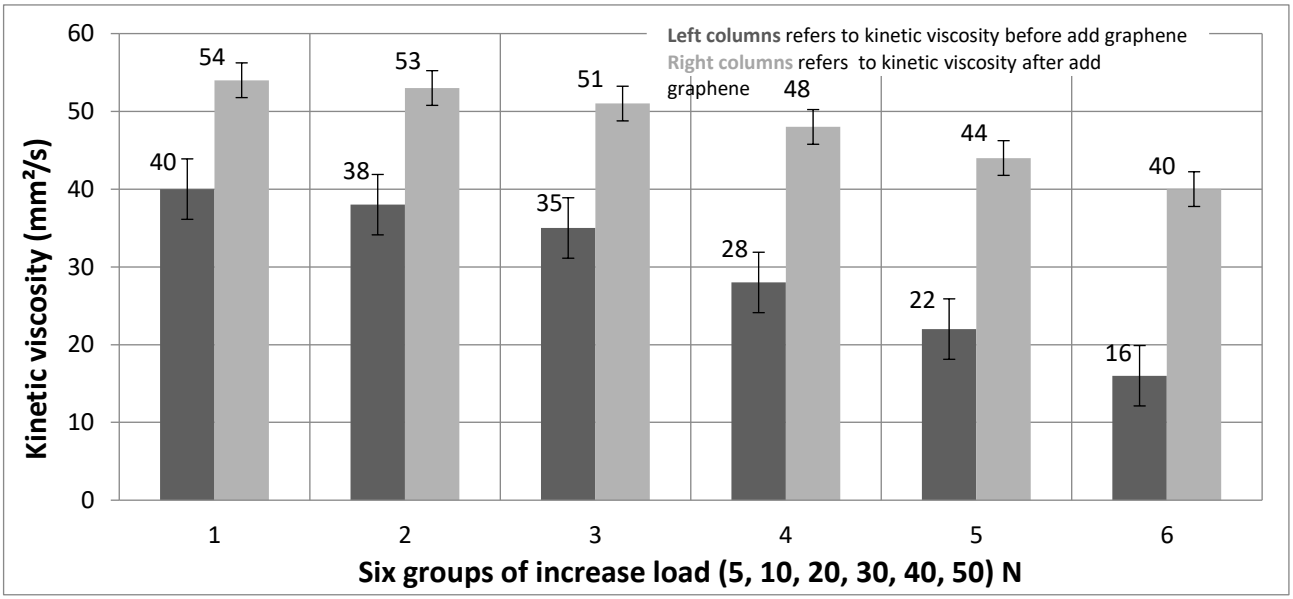


Fig. 25 *Results compare of kinetic viscosity between before and after addition nano-graphene, when raised the load*

5 Conclusions

The findings of this study demonstrate that the two-step preparation method comprising the fabrication of the deep-drawing die, supported by comprehensive DEFORM-based analysis, followed by the formulation of a nanoparticle-enhanced lubricant using graphene-doped SAE-40 oil offers a reliable framework for evaluating advanced tribological performance. The incorporation of nanographene with an approximate particle size of 2 μm represents a promising technological advancement for modern lubrication systems. These additives significantly enhance thermal stability, reduce friction, and improve wear resistance, highlighting their potential for widespread industrial adoption. The investigation of various nanographene concentrations (0, 2, 4, 6, 8, and 10 mg/ml) confirms a pronounced influence on tribological behavior, particularly in terms of wear resistance, friction reduction, and viscosity improvement, even under elevated temperatures above 150 °C and applied loads exceeding 50 N. Among the tested formulations, the lubricant containing 6 mg/ml nanographene with 2% TiO_2 exhibited the most favorable performance, achieving a 43% reduction in wear rate, a 40% decrease in the coefficient of friction, and a 35% increase in kinetic viscosity compared with the baseline lubricant. Although increasing temperature and load intensify wear, friction, and viscosity degradation, the presence of nanographene-based additives effectively mitigates these adverse effects. Furthermore, ANN analysis validated experimental data, confirming strong agreement between measured results and model predictions, and demonstrating the ANN's capability for accurate performance evaluation and error minimization.

5.1 Limitations of the research study

The study was restricted to a small dataset used for ANN development (n = 6 experimental conditions corresponding to graphene concentrations of 0, 2, 4, 6, 8, and 10 mg/ml). The limited dataset was primarily due to the high cost, time requirements, and experimental complexity associated with tribological testing under multiple temperature and load conditions. To mitigate the risk of overfitting, the ANN model incorporated regularization techniques, including dropout and batch normalization, and was validated using LOOCV, which is particularly suitable for very small datasets. The obtained prediction accuracy (R^2 values of 0.847–0.932) indicates that the model successfully captured the underlying relationships within the available data. Nevertheless, the small sample size restricts the statistical robustness and generalizability of the ANN model, and the results should be considered preliminary. Therefore, the ANN is intended primarily as a proof-of-concept predictive tool, and future studies employing substantially larger datasets are required to further validate and improve the model's reliability and applicability to broader operating conditions.

5.2 Recommendations for Future research work

Future research should examine the long-term stability of nanographene-based lubricants, including dispersion durability under continuous loading. Studies using different base oils and hybrid nanoparticle combinations are recommended to optimize performance and broaden applicability. Lifecycle and cost assessments are also needed to evaluate industrial and environmental feasibility. Additionally, advanced surface characterization

methods can provide deeper insight into lubrication mechanisms, while expanding ANN modeling with larger datasets and more advanced AI techniques will improve predictive accuracy for future applications.

References

[1] JIANG, Z., ZHAO, J., XIE, H. (2017). Microforming technology: Theory, simulation and practice (1st ed.). *Academic Press*. ISBN 9780128112120

[2] HOUARI, A., MADANI, K., BENYETTOU, M., KADDOURI, N., BELHOUARI, M., AMROUNE, S., MOHAMAD, B., BENAMAR, B., CHELLIL, A. (2025). Estimation of the stress-intensity factor value in the presence of an adhesive defect for a damaged plate repaired with a composite patch. *Metallofizika i Noveishie Tekhnologii*, 47(1), 103–123.

[3] DAODON, W., SAETANG, V. (2023). Improvement of Frictional Property of AISI D2 Tool Steel Surface against JIS SPFC 980Y Advanced High-Strength Steel by Using Laser Texturing Process. *Lubricants*, 11(2), 68.

[4] KUCLOURYA, T., MUDLIAR, S., JAIN, M. K., THAMBA, N. B. (2021). A review on graphene reinforced composites for ballistic applications. *IOP Conference Series: Materials Science and Engineering*, 1123(1), 012051.

[5] PRASHANTHA KUMAR, H. G., ANTHONY XAVIOR, M. (2014). Graphene reinforced metal matrix composite (GRMMC): A review. *Procedia Engineering*, 97, 1033–1040.

[6] BORAH, M., DAHIYA, M., SHARMA, S., MATHUR, R. B., DHAKATE, S. (2014). Few layer graphene derived from wet ball milling of expanded graphite and few layer graphene based polymer composite. *Materials Focus*, 3.

[7] WANG, X., ZHANG, Y., YIN, Z., SU, Y., ZHANG, Y., CAO, J. (2019). Experimental research on tribological properties of liquid phase exfoliated graphene as an additive in SAE 10W-30 lubricating oil. *Tribology International*, 135, 29–37.

[8] LI, L. ZHOU, M. JIN, L. LIU, L. MO, Y. LI, X. MO, Z. LIU, Z. YOU, S., ZHU, H. (2019) Research Progress of the Liquid-Phase Exfoliation and Stable Dispersion Mechanism and Method of Graphene. *Front. Mater.* 6:325.

[9] WANG, J., ZHUANG, W., YAN, T., LIANG, W., LI, T., ZHANG, L., WEI, X. (2021). Tribological performances of copper perrhenate/graphene nanocomposite as lubricating additive under various temperatures. *Journal of Industrial and Engineering Chemistry*, 100, 296–309.

[10] XIAO, H., LIU, S. (2017). 2D nanomaterials as lubricant additive: A review. *Materials & Design*, 135, 319–332.

[11] HOLMBERG, K., ANDERSSON, P., NYLUND, N.-O., MÄKELÄ, K., ERDEMIR, A. (2014). Global energy consumption due to friction in trucks and buses. *Tribology International*, 78, 94–114.

[12] RESTUCCIA, P., RIGHI, M. C. (2016). Tribochemistry of graphene on iron and its possible role in lubrication of steel. *Carbon*, 106, 118–124.

[13] LI, J., ZENG, X., REN, T., VAN DER HEIDE, E. (2014). The Preparation of Graphene Oxide and Its Derivatives and Their Application in Bio-Tribological Systems. *Lubricants*, 2(3), 137-161.

[14] SUN, J., DU, S. (2019). Application of graphene derivatives and their nanocomposites in tribology and lubrication: A review. *RSC Advances*, 9(69), 40642–40661.

[15] LI, Y., ZHANG, S., DING, Q., FENG, D., QIN, B., HU, L. (2018). Liquid metal as novel lubricant in a wide temperature range from −10 to 800 °C. *Materials Letters*, 215, 140–143.

[16] MOBARK, H. F. H., AL-AZZAWI, A. H., ABID ALI, A. K., MOHAMAD, B. (2024). Comparative tribological analysis of Al-Fe-Si and Al-Fe-Cr based alloys. *Structural Integrity and Life*, 24(3), 386–392.

[17] YANG, Y., JIA, W., MA, L., ZHU, J., WANG, H., HOU, K., WANG, J., YANG, S. (2022). A feasible construction strategy of GO-based hetero-film with long service life at multi-environments: Effective friction transfer application. *Tribology International*, 168, 107455.

[18] PAUL, G., SHIT, S., HIRANI, H., KUILA, T., MURMU, N. C. (2019). Tribological Behavior of Dodecylamine Functionalized Graphene Nanosheets Dispersed Engine Oil Nanolubricants." *Tribology International*, vol. 131, 2019, pp. 605–619.

[19] DONG, H. S., QI, S. J. Realising the Potential of Graphene-Based Materials for Biosurfaces-A Future Perspective." *Biosurface and Biotribology*, vol. 1, no. 4, 2015, pp. 229–248. Elsevier,

[20] KIM, K.-S., LEE, H.-J., LEE, C., LEE, S.-K., JANG, H., AHN, J.-H., KIM, J.-H., LEE, H.-J. (2011). Chemical vapor deposition-grown

graphene: The thinnest solid lubricant. *ACS Nano*, 5(6), 5107–5114.

[21] WU, P., CHEN, X., ZHANG, C., ZHANG, J., LUO, J., ZHANG, J. (2021). Modified graphene as novel lubricating additive with high dispersion stability in oil. *Friction*, 9, 143–154.

[22] ZHANG, L., HE, Y., ZHU, L., YANG, C., NIU, Q., AN, C. (2017). In situ alkylated graphene as oil dispersible additive for friction and wear reduction. *Industrial & Engineering Chemistry Research*, 56(32), 9029–9034.

[23] SPEAR, J. C., EWERS, B. W., BATTEAS, J. D. (2015). 2D-nanomaterials for controlling friction and wear at interfaces. *Nano Today*, 10(3), 301–314.

[24] CHOUHAN, A., MUNGSE, H. P., KHATRI, O. P. (2020). Surface chemistry of graphene and graphene oxide: A versatile route for their dispersion and tribological applications. *Advances in Colloid and Interface Science*, 283, 102215.

[25] SARNO, M., SCARPA, D., SENATORE, A., AHMED ABDALGLIL MUSTAFA, W. (2020). rGO/GO Nanosheets in Tribology: From the State of the Art to the Future Prospective. *Lubricants*, 8(3), 31.

[26] LI, S., LI, Q., CARPICK, R. W., GUMBSCH, P., LIU, X. Z., DING, X., SUN, J., LI, J. (2016). The evolving quality of frictional contact with graphene. *Nature*, 539(7630), 541–545.

[27] VINOTH, A., NIRMAL, K.N., KHEDAR, R., DATTA, S. (2021). Optimizing the Tribological Properties of UHMWPE Nanocomposites-An Artificial Intelligence based approach. In: Akinlabi, E., Ramkumar, P., Selvaraj, M. (eds) Trends in Mechanical and Biomedical Design. *Lecture Notes in Mechanical Engineering. Springer*, Singapore.

[28] DATTA, S., CHATTOPADHYAY, P. P. (2013). Soft computing techniques in advancement of structural metals. *International Materials Reviews*, 58(8), 475–504.

[29] SINHA, A., SIKDAR (DEY), S., CHATTOPADHYAY, P. P., DATTA, S. (2013). Optimization of mechanical property and shape recovery behavior of Ti-(∼49at.%) Ni alloy using artificial neural network and genetic algorithm. *Materials & Design*, 46, 227–234.

[30] BHATTACHARYYA, T., SINGH, S. B., SIKDAR (DEY), S., BHATTACHARYYA, S., BLECK, W., BHATTACHARJEE, D. (2013). Microstructural prediction through artificial neural network (ANN) for development of transformation induced plasticity (TRIP) aided steel. *Materials Science and Engineering*: A, 565, 148–157.

[31] MOHANTY, I., BHATTACHARJEE, D., DATTA, S. (2011). Designing cold rolled IF steel sheets with optimized tensile properties using ANN and GA. *Computational Materials Science*, 50(8), 2331–2337.

[32] HETTIARACHCHI, S. J., BOWEN, J., KERSHAW, M., BARAGAU, I.-A., NICOLAEV, A., KELLICI, S. (2023). Nanostructured Al_2O_3/graphene additive in bio-based lubricant: A novel approach to improve engine performance. *Tribology International*, 186, 108619.

[33] MIAO, X., LIU, S., MA, L., YANG, Y., ZHU, J., LI, Z., WANG, J. (2022). Ti3C2-graphene oxide nanocomposite films for lubrication and wear resistance. *Tribology International*, 167, 107361.

[34] MADKOUR, T. M., FADL, S., DARDIR, M. M., MEKEWI, M. A. (2016). High performance nature of biodegradable polymeric nanocomposites for oil-well drilling fluids. *Egyptian Journal of Petroleum*, 25(2), 281–291.

[35] OMRANI, E., MOGHADAM, A. D., KASAR, A. K., ROHATGI, P., MENEZES, P. L. (2021). Tribological Performance of Graphite Nanoplatelets Reinforced Al and Al/Al2O3 Self-Lubricating Composites. *Materials*, 14(5), 1183.

[36] Zhou, H., Shi, X., Liu, X., Lu, G., Chen, Y. (2019). Tribological properties and self-repairing functionality of Ti6Al4V-multilayer graphene-Ag composites. *Journal of Materials Engineering and Performance*, 28(6), 3381–3392.

[37] WANG, W., HAN, Z., WANG, Q., WEI, B., XIN, S., GAO, Y. (2020). Tribological Properties of Ti2AlNb Matrix Composites Containing Few-Layer Graphene Fabricated by Spark Plasma Sintering. *Metals*, 10(7), 924.

[38] BAO, J., CHEN, G., ZHAO, J., HE, Y., HUANG, Y., LUO, J. (2021). Improvement of the lubrication properties of grease with Mn_3O_4/graphene (Mn_3O_4#G) nanocomposite additive. *Friction*, 9(6), 1361–1377.

[39] RESTUCCIA, P., FERRARIO, M., RIGHI, M. C. (2020). Monitoring water and oxygen splitting at graphene edges and folds: Insights into the lubricity of graphitic materials. *Carbon*, 156, 93–103.

[40] ASM Handbook, "Volume 4A Steel Heat Treating Fundamentals and Processes", 2013.

[41] HALDAR, A., CHATTERJEE, S., KOTIA, A., KUMAR, N., GHOSH, S. K. (2020). Analysis of rheological properties of MWCNT/SiO2 hydraulic oil nanolubricants using regression and artificial neural network. *International Communications in Heat and Mass Transfer*, 116, 104723.

[42] ASTM International. (2004). ASTM G99-04: Standard test method for wear testing with a pin-on-disk apparatus.

[43] SHARUDDIN, M. H. BIN, SULAIMAN, M. H., KAMARUDDIN, S., DAHNEL, A. H., ABD HALIM, N. F. H., RIDZUAN, M. J. M., ABDUL-RANI, A. M. (2023). Properties and tribological evaluation of graphene and fullerene nanoparticles as additives in oil lubrication. Proceedings of the Institution of Mechanical Engineers, Part J: *Journal of Engineering Tribology*, 237(8), 1647–1656.

[44] KUMAR, N., SAINI, V., BIJWE, J. (2020). Tribological investigations of nano and micro-sized graphite particles as an additive in lithium-based grease. *Tribology Letters*, 68, 124.

[45] WANG, Y., LIU, Z., GAO, X., QIU, Q., WANG, M. (2024). Influence of Few-Layer Graphene on Frictional Properties of Lithium Compound Grease. *Coatings*, 14(5), 561.

[46] STEFAN-HENNINGSEN, E., ROBERTS, N., KIANI, A. (2025). Enhancing tribological performance: A comprehensive review of graphene-based additives in lubricating greases. *Results in Engineering*, 25, 104551.

[47] DONG, Y., MA, B., XIONG, C., LIU, Y., ZHAO, Q. (2023). Study on the Lubricating Characteristics of Graphene Lubricants. *Lubricants*, 11(12), 506.

[48] YEHIA, H. M., NOUH, F., EL-KADY, O. (2018). Effect of graphene nano-sheets content and sintering time on the microstructure, coefficient of thermal expansion, and mechanical properties of (Cu/WC–TiC-Co) nano-composites. *Journal of Alloys and Compounds*, 764, 36–43.

[49] ESSA, F. A., ELSHEIKH, A. H., YU, J., ELKADY, O. A., SALEH, B. (2021). Studies on the effect of applied load, sliding speed and temperature on the wear behavior of M50 steel reinforced with Al_2O_3 and/or graphene nanoparticles. *Journal of Materials Research and Technology*, 12, 283–303.

[50] CHAIYASON, T., PRASOMTHONG, S., THOSA, P., CHARONERAT, S., KEIDLAPHI, P. (2026). Hybrid ANN–GA Modeling and Experimental Optimization of GMAW-Based Additive Manufacturing of Aluminum 5083 for Enhanced Mechanical Properties. *Manufacturing Technology Journal*, 26(2), 133-147.

[51] BAJTOŠOVÁ, L., MYŠIČKOVÁ, M., ŠTAFFENOVÁ, N., CHOCHOĽAKOVÁ, E., HANUŠ, J., FIKAR, J., CIESLAR, M. (2025). In Situ TEM and Molecular Dynamics Investigation of Grain Growth in Nanocrystalline Cu Nanoparticles. *Manufacturing Technology Journal*, 25(5), 576-581.

[52] KNAST, P., PETRŮ, J., LEGUTKO, S., SOOS, L., POKUSOVA, M. (2025). SEM Analysis of Surface Layers with Variable Ra Parameters for Tribological Optimization in Design Engineering. *Manufacturing Technology Journal*, 25(2), 185-201.